Synthesis, Characterization, and Antibacterial Activity of ZnO-CuO Nanoparticles Embedded in Chitosan and Polyvinyl Alcohol as Supporting Materials

Ahmad Fatoni[1*], Marcelina Putriani[1], Amar Mulya Lubis[1], Mauizatul Hasanah[1], Ensiwi Munarsih[1], and Nurlisa Hidayati[2]

[1]*Pharmacy Study Program, Sekolah Tinggi Ilmu Farmasi Bhakti Pertiwi, Palembang, Indonesia*
[2]*Department of Chemistry, Faculty of Mathematic and Natural Sciences, Universitas Sriwijaya, Ogan Ilir, Indonesia*

ARTICLE INFO	ABSTRACT
  	The biosynthesis of bimetallic metal nanoparticles (ZnO–CuO) and their interaction with chitosan and polyvinyl alcohol (PVA) have garnered significant attention in recent years, primarily due to their promising antibacterial applications. This work proposes the bio-fabrication of ZnO–CuO nanoparticles, chitosan–PVA–ZnO–CuO nanoparticle films, and reports their physicochemical and antibacterial potential. Green betel leaves (*Piper betle* L.) ethanol extract was used to synthesize ZnO–CuO nanoparticles. For as-prepared bimetallic NPs, chitosan (CS), PVA, and bimetallic NPs-based films were fabricated using the casting technique. The films were investigated by Fourier Transform Infrared (FT-IR) spectroscopy, X-ray Diffraction (XRD), Scanning Electron Microscopy (SEM), and the antibacterial activity was evaluated by the agar diffusion method. FT-IR measurements showed the presence of Zn–O and Cu–O functional groups at 396 cm^{-1} and 418 cm^{-1} in the nanoparticles, and the films A, B, and C, these bands were observed at 394–395 cm^{-1} (Zn–O) and 409–416 cm^{-1} (Cu–O). Crystallite sizes of ZnO, CuO, and ZnO–CuO NPs were 4.845 nm, 54.143 nm, and 5.306 nm, respectively. SEM examination showed that the surface of the films was rough and not homogeneous. Antibacterial experiments revealed the better inhibitory activity of film C than film A and film B. The advantage of the antibacterial property was attributed to the reactive oxygen species (ROS) generated by the ZnO–CuO in collaboration with chitosan. These results indicate that chitosan/PVA film loaded with ZnO–CuO NPs holds great promise as an effective antibacterial packaging material.

INTRODUCTION

Metal nanoparticles (MNPs) are synthesized by cheap and effective biological pieces that can be used in various construction technologies and are of interest to biologists, chemists, and material scientists. A case in point, now on CuO–ZnO NPs of different chemical composition, crystal structure, shape, specific surface area, surface functional chemical groups, etc., can be thus fabricated and utilized to capitalize on greatly enhanced properties, particularly the enhanced bactericidal effect [1].

Over the last 20 years, metal oxide nanoparticles (MNPs) such as copper oxide, zinc oxide, etc. (bimetallic nanoparticles)

have been gaining much attention [2]. A ZnO and CuO nanoparticle bimetallic combination is a subject of interest, as electron–hole pair recombination is fast and is stimulated by UV light only, the photodynamic antibacterial activity of ZnO nanostructures is marginal. CuO is a bio-safe, eco-friendly, and p-type semiconductor material used to enhance the antibacterial activity of ZnO nanostructures. Combining between CuO and ZnO nanostructures can effectively separate the charge carrier and significantly decrease the recombination of electron–hole pairs [3]. When these two metal oxides are mixed, they form a paste with extraordinary characteristics, such as a large specific surface area and extremely high heat stability. The number of active sites on their surface is larger, and they can perform such actions as antibacterial activity more effectively, thus improving their reactivity [4].

The physical methods described in [5] do not involve toxic chemicals and do not require special conditions or costly instruments. Green/eco-friendly synthetic techniques are usually employed instead of conventional industrial synthetic pathways to prevent hazardous substances and minimize costly or sophisticated processes. Compared with the traditional physicochemical methods, these environmentally benign processes offer several advantages of being simple, fast, affordable, low-toxic, and eco-friendly. Methods that stabilize nanoparticles by coating them with nasty chemicals that stick to and stabilize them are also not very green.

Environmentally benign metal oxide nanoparticles have been synthesized with the help of diverse microbes and plants. Plants are relatively cheap and abundant in the environment. The use of green betel leaves (leaves of *Piper betle* L.) as a matrix for generating metal nanoparticles is one such case. Betel leaves contain several secondary metabolites such as flavonoids, terpenoids, tannins, alkaloids, and saponins [7]. As stabilizers and reductants, secondary metabolites could be used in the green synthesis of metallic NPs [8]. A higher concentration of stabilizing and reducing agents inhibits the aggregation of NPs and induces the formation of smaller NPs. Nevertheless, green nanoparticle synthesis methods have several merits over chemical production methods as they are environmentally friendly, cost-effective, reproducible, and enable the production of more stable materials.

To improve antibacterial capability, cetyltrimethylammonium bromide (CTAB), as a representative cationic surfactant, is utilized [9]. In the case of volcanic ash and nano clay, CTAB can act as a modifier, and the composite can also act as an adsorbent [10], [11]. The cationic surfactant in alkaline and extremely acidic conditions shows high surfactant activity, bactericidal activity, and stability [12]. Data in the existing literature suggests that cationic surfactant CTAB is easier to form a larger chain than other surfactants. It consists of three methyl groups that bind to an ammonium head group and a 16-carbon base. CTAB has been added during the biosynthesis of ZnO NPs [13] and preparation of ZnO NPs [14], as well as synthesis of ZnO NPs [15], [16]. This depends on the porosity and the shape of the metal nanoparticles, which are significantly

improved by incorporating CTAB surfactant in the reaction medium [16]. CTAB is a surfactant with a hydrophilic head and hydrophobic tail, which can also be used as a modifying agent for synthesizing metal oxides so that the formed metal oxide nanoparticles have good crystallinity [17]. Nanoscaled materials can be pr   epared with anionic, cationic, and nonionic surfactants. Surfactants can tailor the final product's kinetic growth and corresponding morphologies. The morphology and properties of the materials are also dominated by the expansion of the surfactant molecules upon development [18].

Extracts from plant parts, such as leaves of Eriobotrya japonica [20], leaves of Alchemilla vulgaris [19], Alhagi maurorum, and powdered plant parts, can be used as bioreductants or extracts from *Gliricidia sepium* plant parts for ZnO nanoparticle biosynthesis [21]. As per previous studies, leaves of *Averrhoa carambola* L. [22], *Malva sylvestris* [23], *Ficus religiosa* [24], and *Adhatoda vasica* Nees [25] can also act as bioreductants for the synthesis of CuO nanoparticles. Nanoparticles of mixed-metal oxides can be biosynthesized from plant extracts. Zn^{2+}/Cu^{2+} oxide nanoparticles were also prepared using *Bridelia ferruginea* [26], *Sambucus nigra* L. [6], and *Psidium guajava* L. [27]. According to the surveys above, naturally occurring reducing and templating molecules play a role in the biosynthetic process of metal and bimetallic oxide nanoparticles and contribute to the functionalization of the nanoparticles. Double nanoparticles like ZnO-CuO can be biosynthesized using plant extracts. The findings reported in [28] indicated that ZnO-CuO nanoparticles biosynthesized using *V. arctostaphylos* L. fruit extract can be applied as antibacterial agents against *E. coli* and *S. aureus*.

Chitosan, the second most abundant biopolymer after cellulose, has the potential to be used in preparing eco-friendly alternatives. Since chitosan's molecular structure includes protonated amino groups, it becomes soluble, particularly in water containing hydrochloric or acetic acid. This polymer has been found to have excellent film-forming ability due to its high molecular weight, as well as solubility in slow-evaporation solvents [29]. When metal oxide nanoparticles are incorporated into the chemical structure of chitosan, they form chitosan-metal oxide nanoparticle films with antibacterial activities [13], [27].

Due to its marked physical and chemical features, outstanding film-forming and emulsifying properties, and nontoxicity, PVA is a synthetic water-soluble polymer commonly used in polymer blending [30]. Combining chitosan and PVA would improve the film's mechanical properties [31]. Films prepared from chitosan, synthetic polymers (polyvinyl alcohol; PVA), and metal oxide nanoparticles have also been explored for antibacterial applications [32].

In contrast, little work has been published regarding using inorganic materials (e.g., metal oxide nanoparticles) in PVA and chitosan to produce films. The antibacterial activity of chitosan/PVA/ZnO NPs is higher with an increase in the ZnO particle ratio, as reported in [33]. CuO nanoparticles were well dispersed in a

chitosan/PVA solution to form a composite of chitosan/PVA/CuO nanoparticles. They were subsequently used to remove Pb(II) from the solution because of their large specific surface area and high activity [34]. Owing to its amino groups, the chelating property of chitosan can be used to fabricate organic-inorganic composite films [35] that are applied in antibacterial studies [32]. One approach to extend the surface area of ZnO and ZnO-CuO NPs is to prepare them with chitosan/PVA support materials [32], [36], thus enhancing their features like antibacterial efficacy. The chitosan, PVA, and metal nanoparticles exhibit synergistic interactions.

In the absence of prior reports on the application of CTAB as a capping agent in the biosynthesis of ZnO-CuO nanoparticles, it is expected that incorporating CTAB into the biosynthesis process would lead to ZnO-CuO nanoparticles with improved crystallinity. An increased CTAB concentration resulted in a higher degree of crystallinity in the ZnO nanoparticles [37]. After adding CTAB at pH 7, the crystallite size and particle size for CuO nanoparticles were decreased [16]. The enhanced crystallinity of ZnO NPs was attributed to predominant ROS production [37].

The composite nanoparticles of chitosan, ZnO, and CuO possess antibacterial properties. FT-IR, SEM, and XRD characterized biosynthesized ZnO-CuO nanoparticles. For the film formation of the chitosan-PVA-ZnO-CuO nanoparticles, the blend was cast onto a petri dish and dried at room temperature. FT-IR, XRD, and SEM were used to characterize these films, and their antibacterial activity was reported.

METHODS

1. Materials and Tools

The materials used in this study include sodium hydroxide (NaOH), acetic acid (CH_3COOH), zinc acetate dihydrate ($Zn(CH_3COO)_2 \cdot 2H_2O$), copper sulfate pentahydrate ($CuSO_4 \cdot 5H_2O$), ethanol (CH_3CH_2OH), polyvinyl alcohol (($C_2H_4O)_x$), cetyltrimethylammonium bromide (CTAB, $C_{19}H_{42}BrN$), universal pH indicator paper, and nutrient agar. Chitosan (degree of deacetylation 87%) was obtained from Ocean Fresh, Bandung, West Java, Indonesia. Distilled water (aquadest), *S. aureus*, and *E. coli* were sourced from the developed Microbiology Laboratory, and green betel leaves (*Piper betel* L.) were collected from Palembang, Indonesia.

The equipment includes a hotplate (IKA C-Mag HS7) and a calcination furnace (Carbolite Gero). Characterization was carried out using the following instruments: Shimadzu IRSpirit-X FTIR Spectrophotometer for functional group analysis, scanning electron microscope (SEM, Hitachi SU3500) for surface morphology analysis, X-ray diffraction (XRD, Shimadzu XRD-6000) for crystal structure analysis, and ultraviolet-visible (UV-Vis) spectrophotometer (Genesys 150, Thermo Scientific) for bacterial inoculum preparation.

2. Preparation of Plant Extract

The maceration process was carried out using a previously reported method [32] with slight modifications. Leaves of *Piper betle* L. were washed with tap water, followed

by rinsing with distilled water. The leaves were then air-dried at room temperature (25°C) for seven days. The dried leaves were ground into fine powder. Maceration was performed using 70% (v/v) ethanol, which has been reported as an effective solvent for leaf extraction [39]. A total of 25 g of powdered leaves were macerated with 250 mL of 70% ethanol (ratio 1:10) for 24 hours. After maceration, the extract was filtered to obtain the filtrate. This maceration and filtration process was repeated three times to obtain approximately 750 mL of extract.

3.   Nanoparticle Synthesis

Biosynthesis of ZnO, CuO, and CuO nanoparticles was carried out according to the procedure previously described [32], as outlined in Table 1. In brief, 1.646 g of zinc acetate dihydrate and 0.364 g of CTAB (0.02 M) were dissolved in 50 mL of deionized water in a 250 mL beaker. This solution was mixed with 150 mL of *Piper betle* L. leaf ethanol extract and stirred vigorously on a hotplate (100 rpm) at 70°C for 1 hour. The pH of the mixture at this stage was approximately 5.0–6.0. After 1 hour, 0.5 M NaOH solution was slowly added to adjust the pH to around 10. The resulting precipitate was allowed to settle overnight at room temperature (25°C). The precipitate (ZnO nanoparticles) was then washed thoroughly with distilled water and 70% (v/v) ethanol, dried in a vacuum oven at 70°C for one day, and calcined at 400°C for 2 hours in a muffle furnace.

The same procedure was employed for the synthesis of ZnO-CuO and CuO nanoparticles. A schematic diagram illustrating the biosynthesis process is presented in Figure 1.
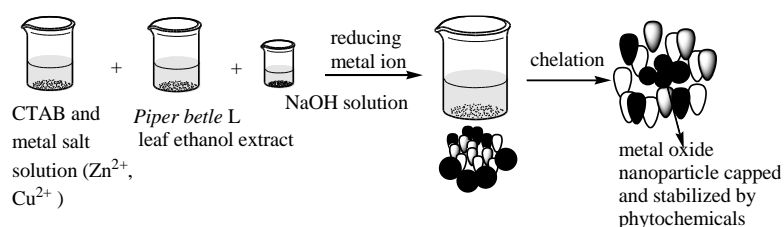

Figure 1. Schematic diagram of biosynthesis of ZnO, CuO, and ZnO-CuO nanoparticles.

4.   Film Fabrication

The film was fabricated following the previously reported method [32]. A 0.1 g chitosan solution was prepared in a 100 mL beaker using 10 mL of an aqueous acetic acid solution (2.5% v/v). The solution was homogenized at 25°C (room temperature) using a hotplate set at 100 °C. Subsequently, 10 mL of chitosan solution was added with 0.1 g of ZnO-CuO nanoparticles, and the mixture was stirred continuously for 1 hour at 25°C (100 rpm). Finally, the solution was added to 10 mL of 2.5% (w/v) PVA solution and stirred for 30 minutes at 25°C (100 rpm). The resulting solution was spread on a Petri plate to form a uniform film and dried at 25°C. After drying (7 days), the film was removed and used for further study. Other films were prepared similarly for comparison purposes. A schematic diagram of the preparation process is presented in Figure 2 and summarized in Table 2.
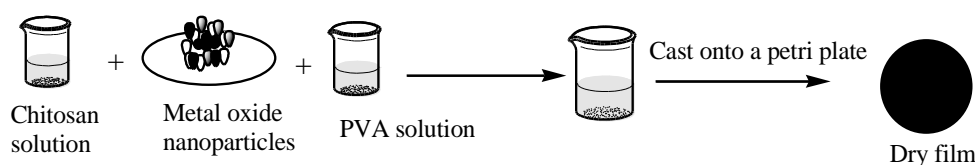
Figure 2. Schematic diagram for film fabrication.

Table 1. The materials for biosynthesis

No	Mass (g) of		Volume of ethanolic extract of *Piper betel* L leaves (mL)	Mass (g) of CTAB	Solution of NaOH 0.5 M (mL)	Product (nanoparticles)
	$Zn(CH_3COO)_2.2H_2O$	$CuSO_4 . 5H_2O$				
1	1.646	-	150	0.364	25	ZnO
2	-	0.624	150	0.364	20	CuO
3	1.646	0.624	150	0.364	25	ZnO-CuO

Table 2. Film composition

No	Chitosan (g)	ZnO-CuO nanoparticles (g)	PVA solution 2.5% w/v (mL)	Film type
1	0.1	0.1	10	A
2	0.2	0.1	10	B
3	0.1	0.2	10	C

5.   Characterization

The ZnO, CuO, ZnO-CuO nanoparticles, and the fabricated films were characterized. Functional groups corresponding to Zn–O and Cu–O bonds were identified using FTIR spectroscopy with the KBr pellet method in the 4000–330 cm^{-1} range. X-ray diffraction (XRD) analysis was conducted using a Cu Kα radiation source (λ = 1.5406 Å) with operating conditions set at 30 kV and 10 mA, in goniometer tube measuring mode. The scan range was from 10° to 90° 2θ with a scan speed of 10.000 deg/min. Surface morphology was observed using a scanning electron microscope (SEM, Hitachi SU3500) operated at 10.0 kV and various magnifications up to ×30,000 (scale bar = 1 μm).

6.   Biological Activities of Film Types A, B, C, Chitosan, and PVA Film

Escherichia coli and *Staphylococcus aureus* were selected as model bacteria to assess the antibacterial activity of the nanoparticles. The bacterial inoculum was prepared by diluting a freshly grown culture with sterile 0.9% NaCl solution, adjusting the optical density (OD) at 580 nm to 25% transmission [40]. The antibacterial activity was evaluated using the agar well diffusion method. After solidification of a 10 mL first layer of nutrient agar on the Petri plate, the second layer containing the microbial inoculum was poured. Films A, B, and C, along with chitosan (negative control), PVA (negative control), and chloramphenicol

solution 0.1% w/v (positive control), were applied onto the plates (film size: approximately 6 mm). The plates were incubated for 24 hours at 37°C [32]. The antibacterial effect was determined by measuring the diameter of the inhibition zone in millimeters using a caliper. The highest inhibition zone observed among the films indicated the strongest antibacterial activity.

RESULTS AND DISCUSSION

1.   Reaction Mechanism for the Formation of ZnO, CuO, and ZnO-CuO Nanoparticles

The major advantage of using plant extracts containing a variety of phytochemicals, as described in [41], is enhancing the in vitro oxidation of metals to metal oxide nanoparticles. A tentative mechanism describing the role of the plant extract in the formation of CuO nanoparticles is as follows: The presence of different phytocomponents such as terpenoids, alkaloids, flavonoids, polyphenols, aldehydes, ketones, sugars, and amides in the plant leaf extract potentially stabilizes and reduces metal ions, thus playing a dual role in nanoparticle synthesis. These phytochemicals reduce the metal salts by chelation into the zero-valent state as a natural process. Polyphenols, with their –OH groups, coordinate with metal ions to form complexes and significantly contribute to nanoparticle formation.

A schematic diagram of this reaction is shown in Figure 3. An interaction is proposed between the micellar solubilized components of the extracts and Zn^{2+} and Cu^{2+} ions at the palisade-Stern layer junction. In the case of CTAB, interactions at the micellar interface were previously reported [42]. The response is accelerated through micelle formation, which enhances the attraction or repulsion between counterions. The proximity of the reacting species at the micellar interface increases molecular collisions. Since micelles are porous and have rough surfaces with water-filled wells, the exact location of the reaction within the micelle remains uncertain; however, localization of reactants at the micelle surface is suggested. Micelle surfaces, being water-enriched, create a non-uniform reaction medium. Upon heating, dissociation of the metal-OH binding occurs, releasing water and initiating the growth of oxide nanoparticles [41]. CTAB plays a significant role in promoting the dispersion of metal oxide nanoparticles and inhibiting their agglomeration, besides affecting micelles and lipophilic biomolecules in the ethanol leaf extract [43].

The formation of ZnO, CuO, and ZnO-CuO nanoparticles was confirmed by observations shown in Figure 4. The synthesis of films A, B, and C is displayed in Figure 5, and their characteristics are summarized and compared with reported values in Table 1.
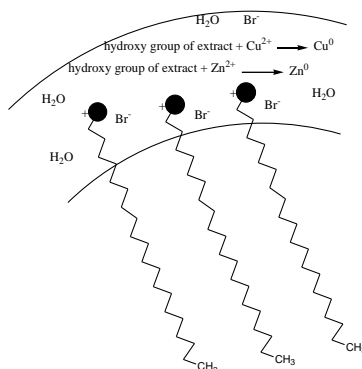
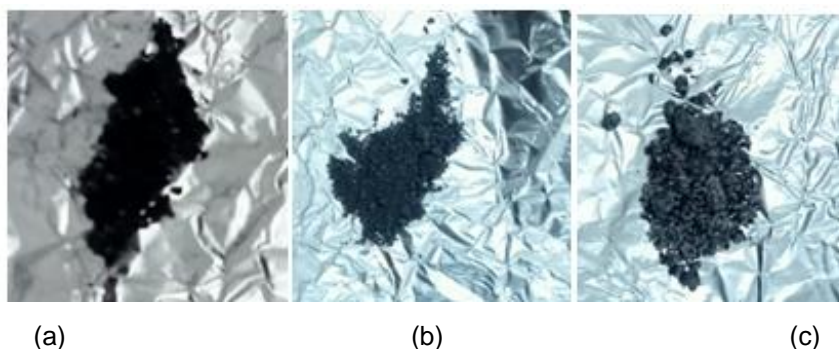**Figure 3.** The process of reducing metal ions by hydroxy groups in the presence of CTAB [42].

(a)   (b)   (c)

Figure 4. Biosynthesis results of ZnO, CuO, and ZnO-CuO nanoparticles.

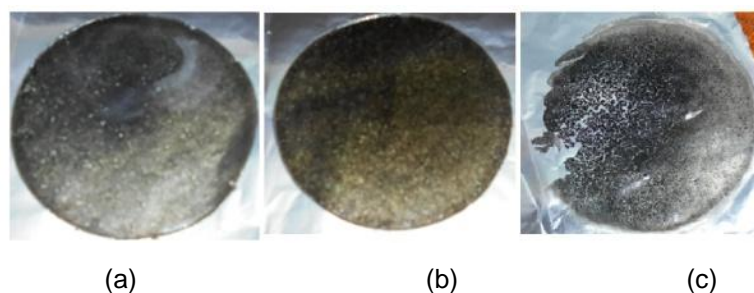(a)   (b)   (c)

Figure 5. The picture of the films A (a), B (b), and C (c).

ZnO and CuO nanoparticles darken in color compared to ZnO-CuO nanoparticles, as shown in Figure 4. The black coloration in the ZnO nanoparticles is attributed to gaps in the crystal structure, where atomic cores of Zn and O interact via Coulomb forces [44].

Digital images of the prepared films are shown in Figure 5. Film B, where the chitosan amount is twice that of the ZnO-CuO nanoparticles, appears darker than films A and C. Film C is lighter compared to B, likely because in film A the ratio of chitosan to ZnO-CuO nanoparticles remained constant, while in film B the chitosan content was increased along with the ZnO-CuO nanoparticle content.

2.   Fourier   Transform   Infrared spectroscopy (FT-IR)

2.1.   *Nanoparticles of ZnO, CuO, and ZnO-CuO*

The FT-IR spectra of nanoparticles of ZnO, CuO, and ZnO-CuO are presented in Figure 6.
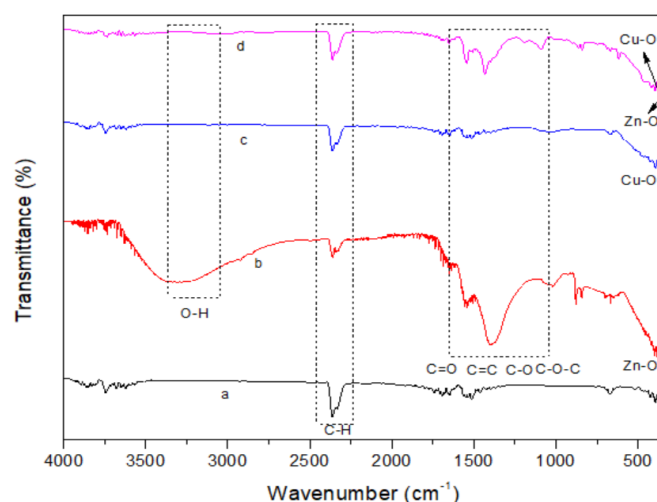
Figure 6. FT-IR spectra of a (CTAB), b (ZnO nanoparticles), cb(CuO nanoparticles), and d (ZnO-CuO nanoparticles).

It can be seen that the strong and broad band centered at 3315–3005 cm^{-1} is due to O–H stretching vibration for phenol or alcoholic functional groups [45] (Figure 6). The C–H stretching and C–H wagging of CTAB were confirmed at 2363–2361 cm^{-1} [46]. The 1700–1000 cm^{-1} range peaks can be attributed to organic residues remaining from the plant (C=C, C=O, C–O, and C–O–C stretching) [21]. The vibration band of metal–oxygen bonds generally appears around 400–700 cm^{-1} in the FTIR spectra of metal oxides. Specifically, Zn–O–Cu–O vibrations were observed at 396 and 418 cm^{-1} [41], [47]; Zn–O bond at 395 cm^{-1} [47]; and Cu–O bond at 421 cm^{-1} [41].

2.2   Film A, B, and C

Figure 7 shows the FTIR spectra of the film structures, and Figure 8 shows the wavenumber positions of the Zn–O and Cu–O groups in films A, B, and C. The FTIR spectra of PVA, chitosan, and films A, B, and C are presented in Figure 7. The bands detected from the chitosan film are 3733 cm^{-1} (O–H/N–H stretching vibration), 2920 cm^{-1} (C–H stretching vibration), 1651 cm^{-1} (amide-I group), and 1557 cm^{-1} (amide-II group) [35] (Figure 7a). The FTIR spectrum of the PVA film (Figure 7b) shows bands as previously discussed.

The FTIR spectra of films A, B, and C (Figure 7c–e) show absorption at 3333 cm^{-1}, 3259 cm^{-1}, and 3236 cm^{-1}, respectively. These bands indicate the overlapping of the stretching vibrations of the –NH and –OH groups of chitosan and PVA films, but with smaller intensities than the original stretching vibrations of chitosan (3733 cm^{-1}) and PVA (3317 cm^{-1}). This shift could be attributed to interactions between the PVA (–OH) and chitosan (–NH$_2$ and –OH) functional groups via hydrogen bonding [48], [49].
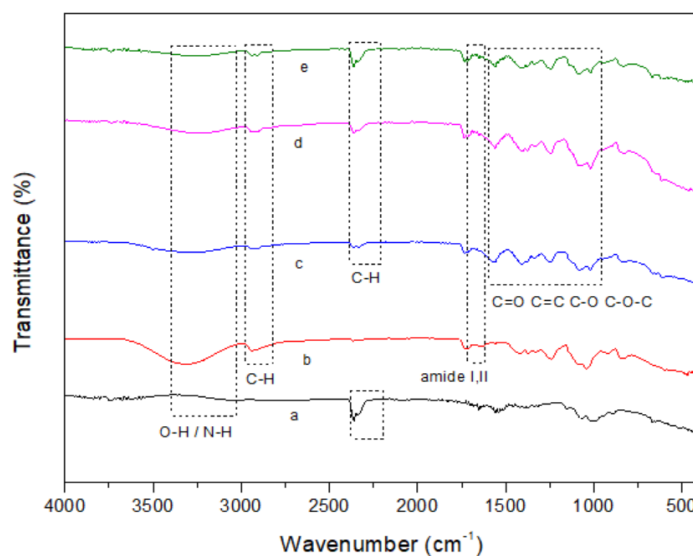
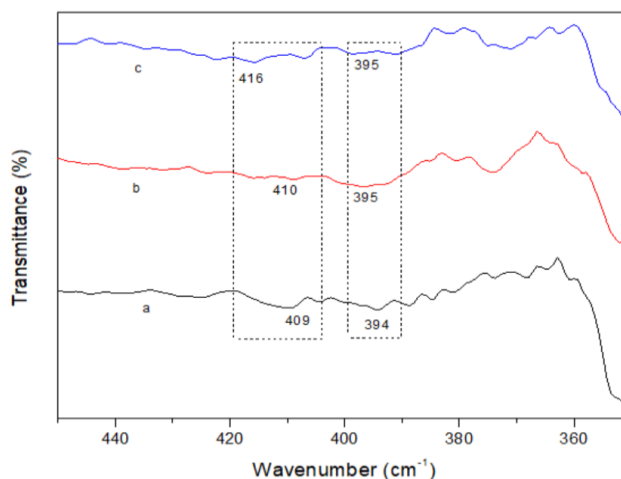**Figure 7.** FT-IR spectra of a (chitosan), b (PVA), c (film A), d (film B) and e (film C).

Figure 8. FT-IR spectra of a (film A), b (film B), and c (film C).

Additionally, the amide-I band in the PVA–chitosan–ZnO–CuO nanoparticle films (A, B, and C) shifted to lower wavenumbers (from 1651 cm^{-1} to 1558–1563 cm^{-1}). As shown in Figure 7, this wavenumber shift reveals hydrogen bonding interactions between the amide-I and reactive functional groups (–NH, –OH) of chitosan with ZnO or CuO nanoparticles (Figure 9) [50], [51].

Zn–O and Cu–O group bands were observed at 394 and 409 cm^{-1} (film A), 395 and 410 cm^{-1} (film B), and 395 and 416 cm^{-1} (film C), respectively (Figure 8). The C–H

stretching vibration of CTAB was observed at 2359 cm^{-1}, 2360 cm^{-1}, and 2361 cm^{-1} in films A, B, and C, respectively. The FTIR spectra of films A, B, and C confirmed the existence of Zn–O and Cu–O groups and well's C–H stretching of CTAB.

Three predominant attractive forces are established between the cationic surfactant and the polymer matrix for CTAB: hydrophobic forces, hydrogen bonding, and electrostatic interactions between the positive charges of the surfactant and negative charges of the polymer matrix [52].
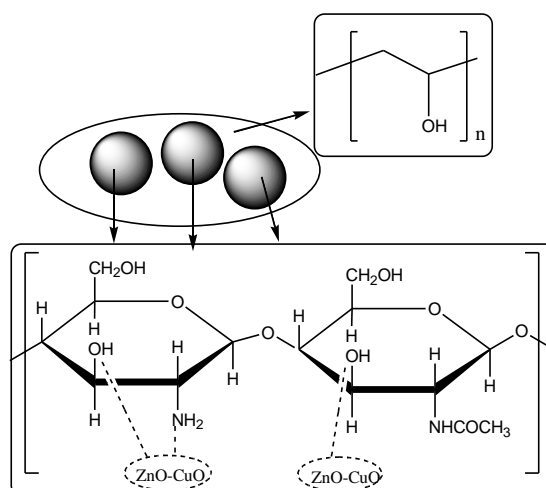
Figure 9. An example of the chemical reaction between ZnO-CuO nanoparticles and chitosan [51]

3. X-Ray diffraction (XRD)

Figure 10 displays the diffractogram of ZnO, CuO, and ZnO-CuO nanoparticles and the diffractogram of film PVA, chitosan, A, B and C are presented in Figure 11. Figure 10a shows the crystalline phase of ZnO nanoparticles calcined at 400 °C. Effective peaks were observed at 32.01°, 34.82°, 36.42°, 47.83°, 56.63°, 62.97°, and 68.16°. These peaks were assigned to the lattice planes (100), (002), (101), (102), (110), (103), (200), and (201) reflections, respectively, confirming the hexagonal wurtzite structure of ZnO [45].

The X-ray diffraction pattern (Figure 10b) confirmed the synthesis of copper-reduced nanoparticles with a copper oxide shell, where major peaks at 2θ were obtained at 32.49°, 35.45°, 38.68°, 48.63°, 58.37°, 61.42°, 67.2°, 74.96°, and 83.57°, attributed to elemental copper. These diffraction peaks are consistent with previous findings [53].

The XRD pattern of ZnO–CuO nanoparticles fabricated with *Piper betle L.* extract is presented in Figure 10c. For ZnO

nanoparticles, peaks appeared at 2θ = 31.90°, 34.61°, 36.38°, 56.59°, and 62.88°. Characteristic peaks of CuO at 2θ = 47.79° and 67.93° were also observed. This demonstrates the coexistence of ZnO and CuO in the ZnO–CuO nanoparticles. When combining the diffractograms with antibacterial consequences, based on toxicity tests, metal oxide nanoparticles with larger texture are more toxic to inflammatory cells compared to smaller and less crystalline ones [38].

Debye Scherrer's formula [21] is used to calculate the crystallite size of nanoparticles, as shown in equation 1.

$$D = (0.9.\lambda / \beta.\cos\theta) \qquad (1)$$

where D is the crystallite size (nm), λ is the X-ray wavelength, β is the full width at half maximum (FWHM), and θ is the Bragg angle. Crystallite sizes of 4.845 nm (ZnO), 5.306 nm (ZnO–CuO), and 54.143 nm (CuO) were estimated.
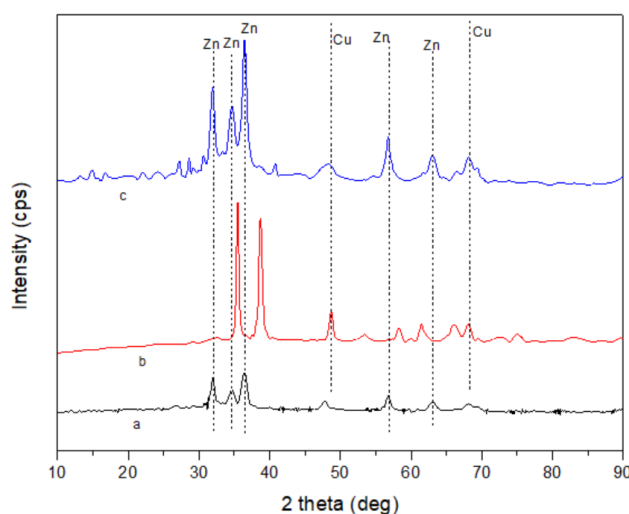
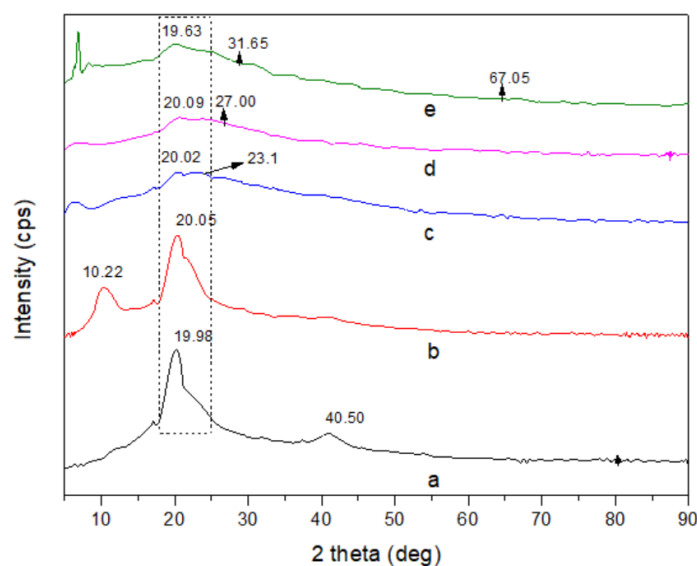**Figure 10.** ZnO (a), CuO (b), and ZnO-CuO nanoparticles (c) diffractograms.

Figure 11. The XRD patern of film PVA (a), chitosan (b), A (a), B (b) and C (c)

The XRD patterns of PVA, chitosan, and PVA–chitosan–ZnO–CuO nanoparticles are presented in Figure 11, comparing films A, B, and C. In pure PVA, two diffraction peaks appeared at 19.98° and 40.50° [54], [55]. Chitosan showed sharp peaks at 2θ values of 10.22° and 20.05°, corresponding to crystal types I and II, respectively [56]. The crystallinity of films A, B, and C is similar to the polymer blend after the addition of ZnO–CuO nanoparticles to the polymer matrix. This is evidenced by a similar diffraction peak that slightly shifts to a lower value with the increasing volume of chitosan (film B) and ZnO–CuO nanoparticles (film C). An intense peak in the 2θ range of 19.63°–20.09° was observed for PVA crystallites in the spectra of films A, B, and C [57].

Each film sample exhibits a distinct diffraction peak at 2θ = 19.63°–20.09°, relating to the semicrystalline state of the polymeric materials used for film formation [58]. The absence of ZnO–CuO nanoparticle-related diffraction peaks in the A and B film

patterns may be due to the low concentration of ZnO–CuO particles undetectable within the chitosan–PVA matrix [57] or due to uniform dispersion of ZnO–CuO nanoparticles. Although a low maximum peak (2θ = 31.65° and 67.05°) was detected, the absence of strong CuO diffraction peaks may result from the high dispersion and embedding of ZnO–CuO nanoparticles within the PVA matrix.

4.   SEM

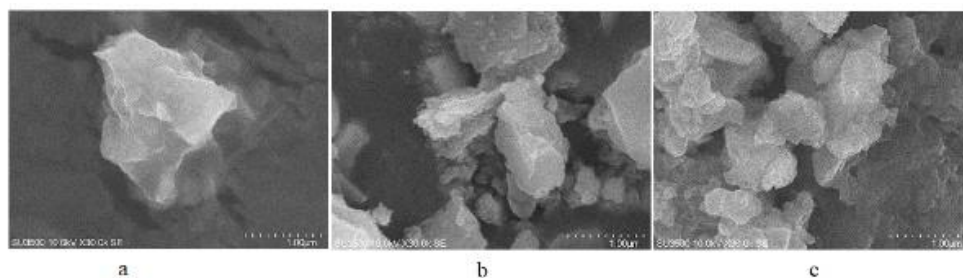Figure 12 shows the surface morphology of ZnO (a), CuO (b), and ZnO-CuO nanoparticles.

Figure 12. SEM images of biosynthesized ZnO (a), CuO (b), and ZnO-CuO nanoparticles (c).
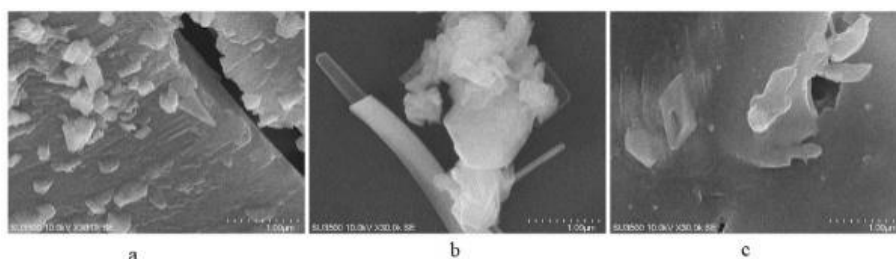
Figure 13. Shows the morphology of synthesized film A (a), B (b), and C (c).

The shape of the biosynthesized ZnO, CuO, and ZnO–CuO nanoparticles is demonstrated in Figure 12, where an irregular monodispersed and near-spherical form is observed. Furthermore, the existence of biomolecules is associated with an even distribution of the particles over the surface, displaying a low percentage of agglomeration or clustered shapes [59].

It is observed in Figure 12 that the introduction of CTAB as the surfactant into the reaction solution leads to products possessing a much larger porosity. CTAB is a long carbon chain that acts as a supplementary fuel—adding more fuel releases more gas, which helps to break down agglomerates to nanoparticles. The particles also grow even after the post-thermal treatment to remove the organics, which is part of the reproduction of the reaction. As observed in the SEM images, the carbon chain of the surfactant serves as a space-filling agent, forming voids during calcination that maintain the porosity of the as-obtained samples [16].

The surface morphologies of film A (a), B (b), and C are shown in Figure 13. The prepared films exhibit roughness and cubical aggregates, as observed in Figures 13a–c. In conformity with previous investigations [32], each film appears rough, with cavities and fractures according to the ZnO–CuO nanoparticle and chitosan mass mix. The inclusion of metal oxide nanoparticles into

biopolymeric matrices provided a reinforcing outcome for mechanical and barrier properties, and their antibacterial activity was considerably enhanced with an increase in the specific surface area [60].

5. Analyze every film for antimicrobial properties

Figure 14 shows the bactericidal properties of each film tested. Table 3 summarizes the calculation of the inhibition zone, as illustrated in Figure 15, while the interaction of the bacteria with the chitosan–ZnO–CuO nanoparticles is shown in Figure 16. The inhibition zones for each film and the mean inhibition zone values for each sample and three replicates are presented.

Table 3 and Figure 15 demonstrate that the mean zone of inhibition of film C is greater than that of films A and B.
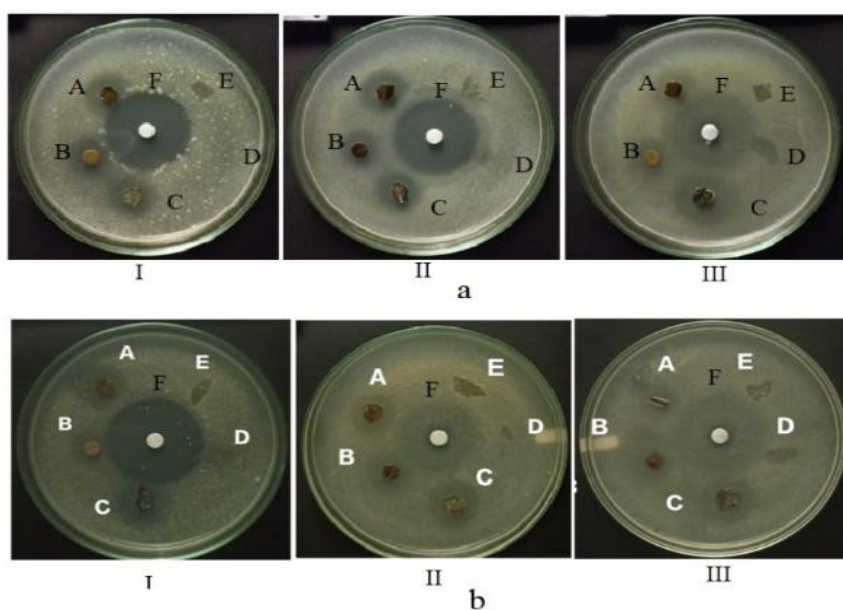

Figure 14. Antibacterial activity test of films A, B, C, D, E, and F by *S aureus* (a) and *E coli* bacteria (b).

The prevention of bacterial growth (even though *S. aureus* cell wall is stronger, more complex, and better protected than *E. coli*) can be influenced by other factors because *E. coli* has a thinner and more sensitive cell wall than *S. aureus* [61]. Smaller nanoparticles might exhibit higher toxicity because more particles are necessary to cover the bacteria and present greater ROS concentrations [62].

The higher generation of reactive oxygen species (ROS) may cause the greater antibacterial activity of ZnO–CuO nanoparticles. A second possible reason may be oxidative stress induced via electron transfer pathways by direct contact of the ZnO–CuO nanocomposite. This electron can be captured and transferred to the dissolved oxygen on the ZnO–CuO nanoparticle due to the high concentration of surface defects. The generation of ROS due to oxygen reduction enhances antibacterial activity [3]. Adding chitosan and bimetallic nanoparticles (ZnO–CuO particles) augmented the antibacterial activities of film C towards *Escherichia coli* and *Staphylococcus aureus*.
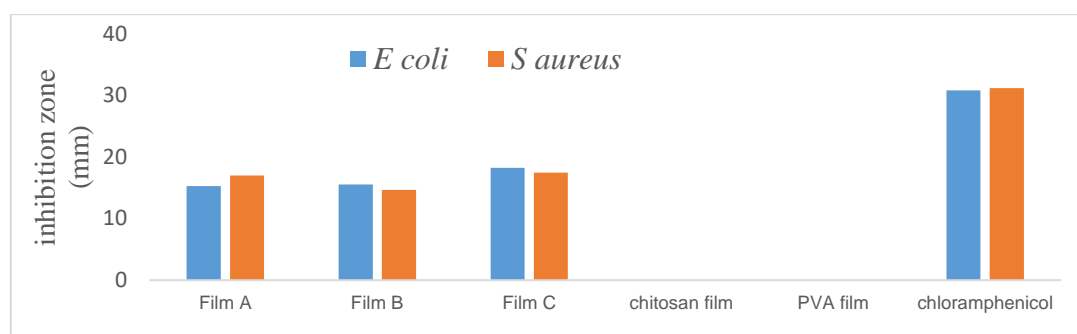
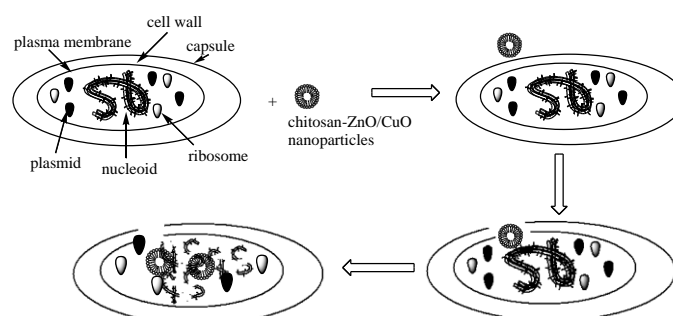**Figure 15.** Bar chart comparison of zones of inhibition

.

Figure 16. The illustration mechanism of the antibacterial activity of chitosan-ZnO-CuO nanoparticles [36].

Changes in the composition and structure of cell membranes, especially cell walls, may reflect variations in antibacterial activity of chitosan–ZnO–CuO nanoparticles against the two types of bacteria under study [36]. The outer membrane of *E. coli* is very thin and soluble, and the periplasmic space, as a mediator between outer and inner membranes, allows diffusional passage to inhibitory chemicals (Figure 16). The present study revealed that the antibacterial activity of ZnO–CuO nanoparticles and chitosan is consistent with previous research [32]. Moreover, the antibacterial activity of chitosan-capped ZnO–CuO nanoparticles was better than in previous studies and is presented in Table 3. These findings reveal the good integration of chitosan–ZnO–CuO nanoparticles.

The results indicated that both tested bacterial strains were sensitive to the antibacterial activity of films A, B, and C against *S. aureus* and *E. coli*. The maximum inhibitory zone was observed in film C (with a chitosan/ZnO–CuO loading ratio of 1:2).

As previously reported [32], chitosan–PVA–metal oxide nanoparticle coatings with a higher weight percentage of metal oxide nanoparticles (ZnO–CuO) exhibit stronger antibacterial activity. A decrease in bacterial viability with increasing concentration of nanoparticles suggests that film C serves better as an antibacterial agent than films A and B. CuO and ZnO nanoparticles were an effective means of delivering toxic species during the exponential phase of bacterial growth, and Cu^{2+} and Zn^{2+} ions were considered the most significant toxic agents [63].

Table 3. The conclusion of every film's antimicrobial evaluation

Petri plate	Inhibition zone (mm)											
	Film A (A)		Film B (B)		Film C (C)		Chitosan Film (D)		PVA film (E)		Chloramphenicol (F)	
	E. coli	*S. aureus*	*E. coli*	*S. aureus*	*E. coli*	*S. aureus*	*E. coli*	*S. aureus*	*E. coli*	*S. aureus*	*E. coli*	*S. aureus*
I	15.2	17.2	12.6	15.6	17.8	16.4	-	-	-	-	33.3.	32.2
II	12.(	18.4	15.5	13.3	17.2	15.6	-	-	-	-	29.6	30.2
III	15.1	15.6	18.6	15.1	19.7	19.55	-	-	-	-	29.5	31.1
Average ± SD	15.3 ± 0.26	17.06 ± 1.40	15.56 ± 3.00	14.66 ± 1.21	18.23 ± 2.17	17.45 ± 2.1	--	-	-	-	30.8 ± 2.17	31.2 ±1.00

The antibacterial activity of chitosan is due to collisions between the positively charged amino groups ($-NH_2$) of chitosan and the negatively charged sections of bacterial cell surfaces. ZnO coated with CuO nanoparticles exhibits functionalities to bind thiol groups (–SH groups), triggering the production of high levels of ROS, and releasing Zn^{2+} from the film, followed by the formation of highly reactive oxygen species (OH^-, H_2O_2, O_2^{2-}). These mechanisms contribute to antibacterial action.

Holes split water into protons and hydroxide ions, and dissolved oxygen is converted into superoxide radical anions ($\cdot O_2^-$), which react with protons to form $HO_2\cdot$ radicals. These radicals collide with electrons to form hydrogen peroxide anions (HO_2^-) [64].

The two main toxic mechanisms of CuO nanoparticles are cellular oxidative stress and dissolution. Extracellular Cu^{2+} and CuO nanoparticles can translocate through the cellular membrane to the cytoplasm via copper transport proteins and endocytosis [65]. This is consistent with previous reports presented in previous studies [32]. As proposed, the morphological and size effects of ZnO and CuO nanoparticles ensure effective cellular uptake against E. coli and S. aureus [66].

CONCLUSION

The ethanolic extract of green betel leaf (*Piper betle* L.) potently synthesizes ZnO–CuO nanoparticles. Applying chitosan and PVA as supporting materials of chitosan–PVA–ZnO–CuO nanoparticle films is possible. Zn–O and Cu–O groups were found in the FTIR spectra of all the films. The ZnO, CuO, and ZnO–CuO nanoparticles possess crystallite physical structures, while all the films exhibit the amorphous nature of their physical structures. The surface morphology of all the films shows a rough structure. All of the films could serve as antibacterial materials. Such films may hold potential for antibacterial packaging applications.

ACKNOWLEDGE

REFERENCES

[1]   M. A. Reyes-Torres *et al.*, "Synthesis of CuO and ZnO nanoparticles by a novel green route: Antimicrobial

activity, cytotoxic effects and their synergism with ampicillin," *Ceram. Int.*, vol. 45, no. 18, pp. 24461–24468, 2019, doi: 10.1016/j.ceramint.2019.08.171.

[2]   B. Kumar, K. Smita, L. Cumbal, A. Debut, and Y. Angulo, "Biofabrication of copper oxide nanoparticles using Andean blackberry (Rubus glaucus Benth.) fruit and leaf," *J. Saudi Chem. Soc.*, vol. 21, pp. S475–S480, 2017, doi: 10.1016/j.jscs.2015.01.009.

[3]   T. Jan *et al.*, "Superior antibacterial activity of ZnO-CuO nanocomposite synthesized by a chemical Co-precipitation approach," *Microb. Pathog.*, vol. 134, no. December 2018, p. 103579, 2019, doi: 10.1016/j.micpath.2019.103579.

[4]   E. Takele, R. Feyisa Bogale, G. Shumi, and G. Kenasa, "Green Synthesis, Characterization, and Antibacterial Activity of CuO/ZnO Nanocomposite Using Zingiber officinale Rhizome Extract," *J. Chem.*, vol. 2023, 2023, doi: 10.1155/2023/3481389.

[5]   S. Kumari *et al.*, "A comprehensive review on various techniques used for synthesizing nanoparticles," *J. Mater. Res. Technol.*, vol. 27, pp. 1739–1763, 2023, doi: 10.1016/j.jmrt.2023.09.291.

[6]   Y. Cao *et al.*, "Green synthesis of bimetallic ZnO–CuO nanoparticles and their cytotoxicity properties," *Sci. Rep.*, vol. 11, no. 1, pp. 1–8, 2021, doi: 10.1038/s41598-021-02937-1.

[7]   L. Heliawati, S. Lestari, U. Hasanah, D. Ajiati, and D. Kurnia, "Phytochemical Profile of Antibacterial Agents from Red Betel Leaf (Piper crocatum Ruiz and Pav) against Bacteria in Dental Caries," *Molecules*, vol. 27, no. 9, 2022, doi: 10.3390/molecules27092861.

[8]   G. Marslin *et al.*, "Secondary metabolites in the green synthesis of metallic nanoparticles," *Materials (Basel).*, vol. 11, no. 6, pp. 1–25, 2018, doi: 10.3390/ma11060940.

[9]   K. Nakata, T. Tsuchido, and Y. Matsumura, "Antimicrobial cationic surfactant, cetyltrimethylammonium bromide, induces superoxide stress in Escherichia coli cells," *J. Appl. Microbiol.*, vol. 110, no. 2, pp. 568–579, 2011, doi: 10.1111/j.1365-2672.2010.04912.x.

[10]   M. Shirzad-Siboni, A. Khataee, A. Hassani, and S. Karaca, "Preparation, characterization and application of a CTAB-modified nanoclay for the adsorption of an herbicide from aqueous solutions: Kinetic and equilibrium studies," *Comptes Rendus Chim.*, vol. 18, no. 2, pp. 204–214, 2015, doi: 10.1016/j.crci.2014.06.004.

[11]   E. T. Wahyuni, R. Roto, F. A. Nissah, Mudasir, and N. H. Aprilita, "Modified silica adsorbent from volcanic ash for Cr(VI) anionic removal," *Indones. J. Chem.*, vol. 18, no. 3, pp. 428–433, 2018, doi: 10.22146/ijc.26905.

[12]   M. A. Akl, A. G. Mostafa, M. Y. Abdelaal, and M. A. K. Nour, "Surfactant supported chitosan for efficient removal of Cr(VI) and anionic food stuff dyes from aquatic solutions," *Sci. Rep.*, vol. 13, no. 1, pp. 1–27, 2023, doi: 10.1038/s41598-023-43034-9.

[13]   A. Fatoni *et al.*, "The Film of Chitosan-ZnO Nanoparticles-CTAB: Synthesis, Characterization and In Vitro Study," *Sci. Technol. Indones.*, vol. 7, no. 1, pp. 58–66, 2022, doi: 10.26554/sti.2022.7.1.58-66.

[14] D. Geetha and T. Thilagavathi, "Hydrothermal synthesis of nano ZnO structures from CTAB," *Dig. J. Nanomater. Biostructures*, vol. 5, no. 2, pp. 297–301, 2010, available online https://www.researchgate.net/publication/266889282_Hydrothermal_synthesis_of_nano_ZnO_structures_from_CTAB.

[15] M. Bazari and N. Najmoddin, "The effect of cationic, anionic and nonionic surfactants on morphology and antibacterial properties of zinc oxide," *Rev. Mater.*, vol. 27, no. 2, 2022, doi: 10.1590/S1517-707620220002.1372.

[16] Z. Singh and I. Singh, "CTAB Surfactant Assisted and High pH Nano-Formulations of CuO Nanoparticles Pose Greater Cytotoxic and Genotoxic Effects," *Sci. Rep.*, vol. 9, no. 1, pp. 1–13, 2019, doi: 10.1038/s41598-019-42419-z.

[17] S. K. Mishra *et al.*, "CTAB mediated synthesis of ZnO nanoparticles: Structural, optical and enhanced blue-green optical emission," *Mater. Today Proc.*, vol. 46, no. May 2022, pp. 2229–2234, 2021, doi: 10.1016/j.matpr.2021.03.481.

[18] H. Siddiqui, M. S. Qureshi, and F. Z. Haque, "Surfactant assisted wet chemical synthesis of copper oxide (CuO) nanostructures and their spectroscopic analysis," *Optik (Stuttg).*, vol. 127, no. 5, pp. 2740–2747, 2016, doi: 10.1016/j.ijleo.2015.11.220.

[19] S. Rajendrachari, P. Taslimi, A. C. Karaoglanli, O. Uzun, E. Alp, and G. K. Jayaprakash, "Photocatalytic degradation of Rhodamine B (RhB) dye in waste water and enzymatic inhibition study using cauliflower shaped ZnO nanoparticles synthesized by a novel One-pot green synthesis method," *Arab. J. Chem.*, vol. 14, no. 6, p. 103180, 2021, doi: 10.1016/j.arabjc.2021.103180.

[20] A. Nazir *et al.*, "Zinc oxide nanoparticles fabrication using Eriobotrya japonica leaves extract: Photocatalytic performance and antibacterial activity evaluation," *Arab. J. Chem.*, vol. 14, no. 8, p. 103251, 2021, doi: 10.1016/j.arabjc.2021.103251.

[21] A. Chinnathambi and T. A. Alahmadi, "Zinc nanoparticles green-synthesized by Alhagi maurorum leaf aqueous extract: Chemical characterization and cytotoxicity, antioxidant, and anti-osteosarcoma effects," *Arab. J. Chem.*, vol. 14, no. 4, p. 103083, 2021, doi: 10.1016/j.arabjc.2021.103083.

[22] A. Fatoni, A. C. Paramita, B. Untari, and N. Hidayati, "Chitosan- CuO Nanopartikel sebagai antibakteri Shigella dysenteriae :Sintesis , Karakterisasi, dan Studi In Vitro," *JKSA.*, vol. 23, pp. 432–439, 2020, available online: https://ejournal.undip.ac.id/index.php/ksa/article/view/32071

[23] S. Y. Sharaf Zeebaree, A. Y. Sharaf Zeebaree, O. I. Haji Zebari, and A. Y. Sharaf Zebari, "Sustainable fabrication, optical properties and rapid performance of bio-engineered copper nanoparticles in removal of toxic methylene blue dye in an aqueous medium," *Curr. Res. Green Sustain. Chem.*, vol. 4, no. December 2020, p. 100103, 2021, doi: 10.1016/j.crgsc.2021.100103.

[24] B. P. G and X. T. S, "A critical green biosynthesis of novel CuO/C porous nanocomposite via the aqueous leaf extract of Ficus religiosa and their antimicrobial, antioxidant, and adsorption properties," *Chem. Eng. J. Adv.*, vol. 8, p. 100152, 2021, doi:

10.1016/j.ceja.2021.100152.

[25] P. G. Bhavyasree and T. S. Xavier, "Green synthesis of Copper Oxide/Carbon nanocomposites using the leaf extract of Adhatoda vasica Nees, their characterization and antimicrobial activity," *Heliyon*, vol. 6, no. 2, p. e03323, 2020, doi: 10.1016/j.heliyon.2020.e03323.

[26] E. Gurgur, S. S. Oluyamo, A. O. Adetuyi, O. I. Omotunde, and A. E. Okoronkwo, "Green synthesis of zinc oxide nanoparticles and zinc oxide–silver, zinc oxide–copper nanocomposites using Bridelia ferruginea as biotemplate," *SN Appl. Sci.*, vol. 2, no. 5, pp. 1–12, 2020, doi: 10.1007/s42452-020-2269-3.

[27] A. Fatoni, A. Rendowati, L. Sirumapea, L. Miranti, S. Masitoh, and N. Hidayati, "Synthesis, Characterization of Chitosan-ZnO/CuO Nanoparticles Film, and its Effect as an Antibacterial Agent of Escherichia coli," *Sci. Technol. Indones.*, vol. 8, no. 3, pp. 373–381, 2023, doi: 10.26554/sti.2023.8.3.373-381.

[28] R. Mohammadi-Aloucheh, A. Habibi-Yangjeh, A. Bayrami, S. Latifi-Navid, and A. Asadi, "Enhanced anti-bacterial activities of ZnO nanoparticles and ZnO/CuO nanocomposites synthesized using Vaccinium arctostaphylos L. fruit extract," *Artif. Cells, Nanomedicine Biotechnol.*, vol. 46, no. sup1, pp. 1200–1209, 2018, doi: 10.1080/21691401.2018.1448988.

[29] H. Wang, J. Qian, and F. Ding, "Emerging Chitosan-Based Films for Food Packaging Applications," *J. Agric. Food Chem.*, vol. 66, no. 2, pp. 395–413, 2018, doi: 10.1021/acs.jafc.7b04528.

[30] A. Abraham, P. A. Soloman, and V. O. Rejini, "Preparation of Chitosan-Polyvinyl Alcohol Blends and Studies on Thermal and Mechanical Properties," *Procedia Technol.*, vol. 24, pp. 741–748, 2016, doi: 10.1016/j.protcy.2016.05.206.

[31] D. fadia Zatalini, E. Hendradi, Philip Drake, and R. Sari, "The Effect of Chitosan and Polyvinyl Alcohol Combination on Physical Characteristics and Mechanical Properties of Chitosan-PVA-Aloe vera Film," *J. Farm. Dan Ilmu Kefarmasian Indones.*, vol. 10, no. 2, pp. 151–161, 2023, doi: 10.20473/jfiki.v10i22023.151-161.

[32] A. Fatoni *et al.*, "Synthesis, Characterization of Polyvinyl Alcohol-Chitosan-ZnO/CuO Nanoparticles Film and Its Biological Evaluation as An Antibacterial Agent of Staphylococcus aureus," *al-Kimiya*, vol. 10, no. 1, pp. 1–12, 2023, doi: 10.15575/ak.v10i1.24725.

[33] Z. I. Abdeen, A. F. El Farargy, and N. A. Negm, "Nanocomposite framework of chitosan/polyvinyl alcohol/ZnO: Preparation, characterization, swelling and antimicrobial evaluation," *J. Mol. Liq.*, vol. 250, pp. 335–343, 2018, doi: 10.1016/j.molliq.2017.12.032.

[34] X. Jiao, Y. Gutha, and W. Zhang, "Application of chitosan/poly(vinyl alcohol)/CuO (CS/PVA/CuO) beads as an adsorbent material for the removal of Pb(II) from aqueous environment," *Colloids Surfaces B Biointerfaces*, vol. 149, pp. 184–195, 2017, doi: 10.1016/j.colsurfb.2016.10.024.

[35] R. A. Krishnan, O. Mhatre, J. Sheth, S. Prabhu, R. Jain, and P. Dandekar, "Synthesis of zinc oxide nanostructures using orange peel oil

for fabricating chitosan-zinc oxide composite films and their antibacterial activity," *J. Polym. Res.*, vol. 27, no. 8, 2020, doi: 10.1007/s10965-020-2033-9.

[36] A. Aouadi *et al.*, "Introducing the antibacterial and photocatalytic degradation potentials of biosynthesized chitosan, chitosan–ZnO, and chitosan–ZnO/PVP nanoparticles," *Sci. Rep.*, vol. 14, no. 1, pp. 1–29, 2024, doi: 10.1038/s41598-024-65579-z.

[37] S. Abdi and D. Dorranian, "Effect of CTAB concentration on the properties of ZnO nanoparticles produced by laser ablation method in CTAB solution," *Opt. Laser Technol.*, vol. 108, pp. 372–377, 2018, doi: 10.1016/j.optlastec.2018.07.009.

[38] A. A. Selim, A. Al-Sunaidi, and N. Tabet, "Effect of the surface texture and crystallinity of ZnO nanoparticles on their toxicity," *Mater. Sci. Eng. C*, vol. 32, no. 8, pp. 2356–2360, 2012, doi: 10.1016/j.msec.2012.07.007.

[39] B. Vongsak, P. Sithisarn, S. Mangmool, S. Thongpraditchote, Y. Wongkrajang, and W. Gritsanapan, "Maximizing total phenolics, total flavonoids contents and antioxidant activity of Moringa oleifera leaf extract by the appropriate extraction method," *Ind. Crops Prod.*, vol. 44, pp. 566–571, 2013, doi: 10.1016/j.indcrop.2012.09.021.

[40] I. Isnaeni, E. Hendradi, and N. Z. Zettira, "Inhibitory effect of roselle aqueous extracts-HPMC 6000 gel on the growth of staphylococcus aureus ATCC 25923," *Turkish J. Pharm. Sci.*, vol. 17, no. 2, pp. 190–196, 2020, doi: 10.4274/tjps.galenos.2019.88709.

[41] A. Roselyn Maheo, B. Scholastica Mary Vithiya, T. Augustine Arul Prasad, P. Tamizhdurai, and V. L. Mangesh, "Biosynthesis, characterization, biological and photo catalytic investigations of Elsholtzia blanda and chitosan mediated copper oxide nanoparticles: Biosynthesis, characterization, biological and photo catalytic investigations," *Arab. J. Chem.*, vol. 15, no. 3, p. 103661, 2022, doi: 10.1016/j.arabjc.2021.103661.

[42] S. A. Al-Thabaiti, A. Y. Obaid, S. Hussain, and Z. Khan, "Shape-directing role of cetyltrimethylammonium bromide on the morphology of extracellular synthesis of silver nanoparticles," *Arab. J. Chem.*, vol. 8, no. 4, pp. 538–544, 2015, doi: 10.1016/j.arabjc.2014.11.030.

[43] L. Gan, Z. Lu, D. Cao, and Z. Chen, "Effects of cetyltrimethylammonium bromide on the morphology of green synthesized Fe3O4 nanoparticles used to remove phosphate," *Mater. Sci. Eng. C*, vol. 82, no. August 2017, pp. 41–45, 2018, doi: 10.1016/j.msec.2017.08.073.

[44] J. León-Flores *et al.*, "Black ZnO nanoparticles synthesized by a green chemistry process," *Nano Express*, vol. 5, no. 1, 2024, doi: 10.1088/2632-959X/ad1d01.

[45] T. Safawo, B. V. Sandeep, S. Pola, and A. Tadesse, "Synthesis and characterization of zinc oxide nanoparticles using tuber extract of anchote (Coccinia abyssinica (Lam.) Cong.) for antimicrobial and antioxidant activity assessment," *OpenNano*, vol. 3, no. August, pp. 56–63, 2018, doi: 10.1016/j.onano.2018.08.001.

[46] F. Asadi, H. Forootanfar, and M. Ranjbar, "A facile one-step preparation of Ca10(PO4)6(OH)2/Li-

BioMOFs resin nanocomposites with Glycyrrhiza glabra (licorice) root juice as green capping agent and mechanical properties study," *Artif. Cells, Nanomedicine Biotechnol.*, vol. 48, no. 1, pp. 1331–1339, 2020, doi: 10.1080/21691401.2020.1842748.

[47] Y. H. I. Mohammed *et al.*, "Green Synthesis of Zinc Oxide Nanoparticles Using Cymbopogon citratus Extract and Its Antibacterial Activity," *ACS Omega*, vol. 8, no. 35, pp. 32027–32042, 2023, doi: 10.1021/acsomega.3c03908.

[48] Annu, A. Ali, and S. Ahmed, "Eco-friendly natural extract loaded antioxidative chitosan/polyvinyl alcohol based active films for food packaging," *Heliyon*, vol. 7, no. 3, p. e06550, 2021, doi: 10.1016/j.heliyon.2021.e06550.

[49] D. S. Vicentini, A. Smania, and M. C. M. Laranjeira, "Chitosan/poly (vinyl alcohol) films containing ZnO nanoparticles and plasticizers," *Mater. Sci. Eng. C*, vol. 30, no. 4, pp. 503–508, 2010, doi: 10.1016/j.msec.2009.01.026.

[50] E. Prokhorov, G. Luna-Bárcenas, J. M. Y. Limón, A. G. Sánchez, and Y. Kovalenko, "Chitosan-zno nanocomposites assessed by dielectric, mechanical, and piezoelectric properties," *Polymers (Basel).*, vol. 12, no. 9, pp. 1–14, 2020, doi: 10.3390/polym12091991.

[51] K. Santiago-Castillo *et al.*, "Effect on the processability, structure and mechanical properties of highly dispersed in situ ZnO:CS nanoparticles into PVA electrospun fibers," *J. Mater. Res. Technol.*, vol. 11, pp. 929–945, 2021, doi: 10.1016/j.jmrt.2021.01.049.

[52] A. Bibi, S. U. Rehman, R. Faiz, T. Akhtar, M. Nawaz, and S. Bibi, "Effect of surfactants on swelling capacity and kinetics of alginate-chitosan/CNTs hydrogel," *Mater. Res. Express*, vol. 6, no. 8, 2019, doi: 10.1088/2053-1591/ab0697.

[53] L. A. Kolahalam, K. R. S. Prasad, P. M. Krishna, N. Supraja, and S. Shanmugan, "The exploration of bio-inspired copper oxide nanoparticles: synthesis, characterization and in-vitro biological investigations," *Heliyon*, vol. 8, no. 6, p. e09726, 2022, doi: 10.1016/j.heliyon.2022.e09726.

[54] S. Rajan, K. Marimuthu, C. B. Ayyanar, and M. E. Hoque, "Development and in-vitro characterization of HAP blended PVA/PEG bio-membrane," *J. Mater. Res. Technol.*, vol. 18, pp. 4956–4964, 2022, doi: 10.1016/j.jmrt.2022.04.130.

[55] M. Jha and N. G. Shimpi, "Mechanical response of silver/polyvinyl alcohol thin film: From one-step and cyclic nanoindentation," *Adv. Ind. Eng. Polym. Res.*, vol. 5, no. 3, pp. 159–170, 2022, doi: 10.1016/j.aiepr.2021.11.001.

[56] J. Yan, J. Xu, S. Ai, K. Zhang, F. Yang, and Y. Huang, "Degradation of chitosan with self-resonating cavitation," *Arab. J. Chem.*, vol. 13, no. 6, pp. 5776–5787, 2020, doi: 10.1016/j.arabjc.2020.04.015.

[57] A. M. Pandele, M. Ionita, L. Crica, E. Vasile, and H. Iovu, "Novel Chitosan-poly(vinyl alcohol)/graphene oxide biocomposites 3D porous scaffolds," *Compos. Part B Eng.*, vol. 126, pp. 81–87, 2017, doi: 10.1016/j.compositesb.2017.06.010.

[58] M. T. Khorasani, A. Joorabloo, A. Moghaddam, H. Shamsi, and Z. MansooriMoghadam, "Incorporation

of ZnO nanoparticles into heparinised polyvinyl alcohol/chitosan hydrogels for wound dressing application," *Int. J. Biol. Macromol.*, vol. 114, no. 2017, pp. 1203–1215, 2018, doi: 10.1016/j.ijbiomac.2018.04.010.

[59] T. A. Orshiso *et al.*, "Biosynthesis of Artemisia abyssinica Leaf Extract-Mediated Bimetallic ZnO-CuO Nanoparticles: Antioxidant, Anticancer, and Molecular Docking Studies," *ACS Omega*, vol. 8, no. 44, pp. 41039–41053, 2023, doi: 10.1021/acsomega.3c01814.

[60] J. L. Castro-Mayorga, M. J. Fabra, A. M. Pourrahimi, R. T. Olsson, and J. M. Lagaron, "The impact of zinc oxide particle morphology as an antimicrobial and when incorporated in poly(3-hydroxybutyrate-co-3-hydroxyvalerate) films for food packaging and food contact surfaces applications," *Food Bioprod. Process.*, vol. 101, pp. 32–44, 2017, doi: 10.1016/j.fbp.2016.10.007.

[61] T. Zhu, S. Fu, W. Xie, F. Li, and Y. Liu, "Comparison of inactivation characteristics of Escherichia coli and Staphylococcus aureus in water by rotary plasma jet sterilization," *Environ. Technol. Innov.*, vol. 36, p. 103746, 2024, doi: 10.1016/j.eti.2024.103746.

[62] B. Lallo da Silva, B. L. Caetano, B. G. Chiari-Andréo, R. C. L. R. Pietro, and

L. A. Chiavacci, "Increased antibacterial activity of ZnO nanoparticles: Influence of size and surface modification," *Colloids Surfaces B Biointerfaces*, vol. 177, no. September 2018, pp. 440–447, 2019, doi: 10.1016/j.colsurfb.2019.02.013.

[63] R. Dadi, R. Azouani, M. Traore, C. Mielcarek, and A. Kanaev, "Antibacterial activity of ZnO and CuO nanoparticles against gram positive and gram negative strains," *Mater. Sci. Eng. C*, vol. 104, no. March, p. 109968, 2019, doi: 10.1016/j.msec.2019.109968.

[64] A. Al Baroot, M. Alheshibri, Q. A. Drmosh, S. Akhtar, E. Kotb, and K. A. Elsayed, "A novel approach for fabrication ZnO/CuO nanocomposite via laser ablation in liquid and its antibacterial activity: A novel approach for fabrication ZnO/CuO nanocomposite," *Arab. J. Chem.*, vol. 15, no. 2, p. 103606, 2022, doi: 10.1016/j.arabjc.2021.103606.

[65] J. Hou, X. Wang, T. Hayat, and X. Wang, "Ecotoxicological effects and mechanism of CuO nanoparticles to individual organisms," *Environ. Pollut.*, vol. 221, pp. 209–217, 2017, doi: 10.1016/j.envpol.2016.11.066.

[66] R. B. Asamoah *et al.*, "Synthesis and characterization of zinc and copper oxide nanoparticles and their antibacteria activity," *Results Mater.*, vol. 7, no. April, p. 100099, 2020, doi: 10.1016/j.rinma.2020.100099.